The Solid State Conversion Reaction of Epitaxial $FeF_2(110)$ Thin Films with Lithium Studied by Angle-Resolved X-Ray Photoelectron Spectroscopy: Supporting Information

Ryan Thorpe,* Sylvie Rangan, and Robert A. Bartynski†
Department of Physics and Astronomy and Laboratory for Surface Modification, Rutgers University, 136 Frelinghuysen Road, Piscataway, New Jersey 08854, United States

Ryan Whitcomb
Department of Applied Physics, University of Michigan, 450 Church Street, Ann Arbor, MI 48109, United States

Ali C. Basaran, Thomas Saerbeck,‡ and Ivan K. Schuller
Department of Physics and Center for Advanced Nanoscience, University of California San Diego, 9500 Gilman Drive, La Jolla, CA 92093, United States

SI. HELIUM ION MICROSCOPY OF THE IRON FLUORIDE FILM

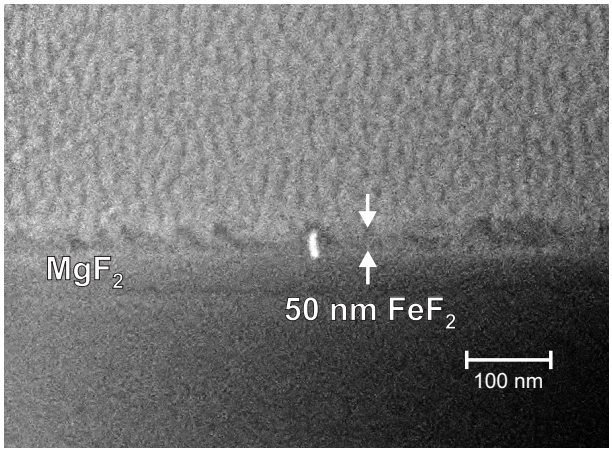

FIG. S1: Helium Ion Microscope image of the as-grown $FeF_2(110)$ thin film showing 10-15 nm lateral domain size and a film thickness of $\sim$ 50 nm.

Figure S1 shows an image of the as-grown $FeF_2(110)$ film as taken by a Zeiss ORION Helium-Ion Microscope (HIM) operating at an accelerating voltage of 35 kV, a beam current of 1 pA, and a 1 μs dwell time. During imaging, the sample surface was oriented at a 45° angle with respect to the ion beam in order to simultaneously image the surface and cross section of the film. Three distinct regions are visible in this image: a textured region at the top of the image, a narrow band in the center, and a uniform layer at the bottom. These features are attributed to the $FeF_2(110)$ surface (with $<$ 1 nm corrugations), the bulk FeF_2 layer, and the MgF_2 substrate respectively. This image confirms that the FeF_2 film is about 50 nm in thickness and suggests that the film is composed of 10-15 nm domains.

SII. IDENTIFICATION OF IRON CHEMICAL SPECIES

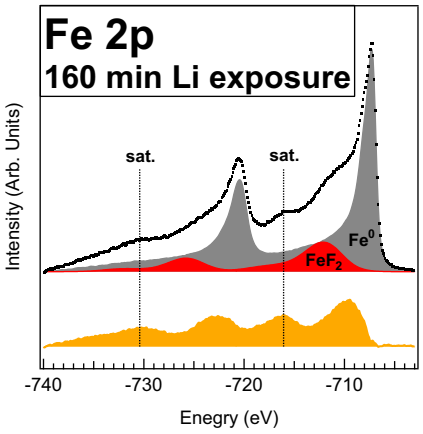

FIG. S2: Fe 2p XPS spectrum of the $FeF_2(110)$ sample after 160 minutes of total Li exposure. The satellite features of the $Fe_xLi_{2-2x}F_2$ component are clearly visible, and are not fit by any combination of iron fluoride or oxide reference spectra.

Figure S2 shows a Fe 2p core level spectrum obtained from the FeF_2 surface after exposure to atomic Li for 160 minutes. The Fe 2p spectral components arising from FeF_2 and Fe^0 were both taken from reference spectra, and were not sufficient to fit the data. In particular, the presence of the satellite features at binding energies of -716 eV and -730 eV, labeled in Figure S2 was not consistent with any known iron fluoride or oxide species.[1–4] An additional component was then constructed, and subsequently identified as $Fe_xLi_{2-2x}F_2$, using the Fe 2p spectrum taken after the final Li exposure (160 min), as shown in Figure S2. This was chosen as the spectrum with the highest ratio of $Fe_xLi_{2-2x}F_2$:FeF_2.

Identification of the $Fe_xLi_{2-2x}F_2$ component was accomplished via comparisons with previous studies. Ko and coworkers have previously observed an expansion in the LiF rock salt lattice upon delithiation of an

FeF_2 cathode.[5] This was attributed to the formation of $Fe_xLi_{2-2x}F_2$.

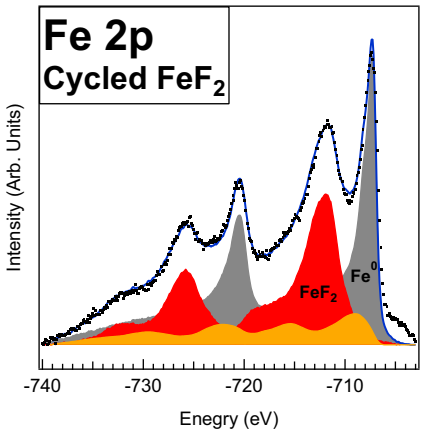

FIG. S3: Fe 2p XPS spectrum from a cycled FeF_2 cathode showing the same spectral components as the thin film sample.[6]

The formation of $Fe_xLi_{2-2x}F_2$ was also observed in recent *ex situ* XPS measurements of electrochemically cycled FeF_2 electrodes.[6] Figure S3 shows the peak fitting scheme used for a delithiated electrode in this previous work. These measurements showed that the $Fe_xLi_{2-2x}F_2$ did not fully dissociate upon the delithiation of the electrode, and hence this ternary compound might be partially responsible for the capacity losses observed in FeF_2 cells.

SIII. EVOLUTION OF IRON PEAKS

The reduction of the FeF_2 film upon exposure to lithium was quantified by fitting the Fe 2p peak with a sum of Fe^0, FeF_2, and $Fe_xLi_{2-2x}F_2$ components. Figure S4 shows the evolution of the normal emission Fe 2p spectra for several different lithium exposures. The spectra have been normalized by their maximum intensities in order to highlight their visual differences. From these spectra, it can be seen that the relative intensities of the Fe^0 and $Fe_xLi_{2-2x}F_2$ components increase monotonically as a function of lithium exposure, while the FeF_2 intensity simultaneously decreases. The Fe:$Fe_xLi_{2-2x}F_2$ ratio increases slightly as a function of exposure, from 0.85 after 5 minutes of exposure to 1.10 after 160 minutes.

SIV. ARXPS DETAILS

The model used to fit the $R(\theta, d)$ curves consisted of an infinitely thick film of FeF_2 with an inhomogeneously thick overlayer of $Fe_xLi_{2-2x}F_2$ and Fe metal, as shown in Figure S5. In order to model the attenuation of the FeF_2 photoelectrons, the overlayer was divided vertically into four different types of regions: (1) thick Fe^0, (2) thick

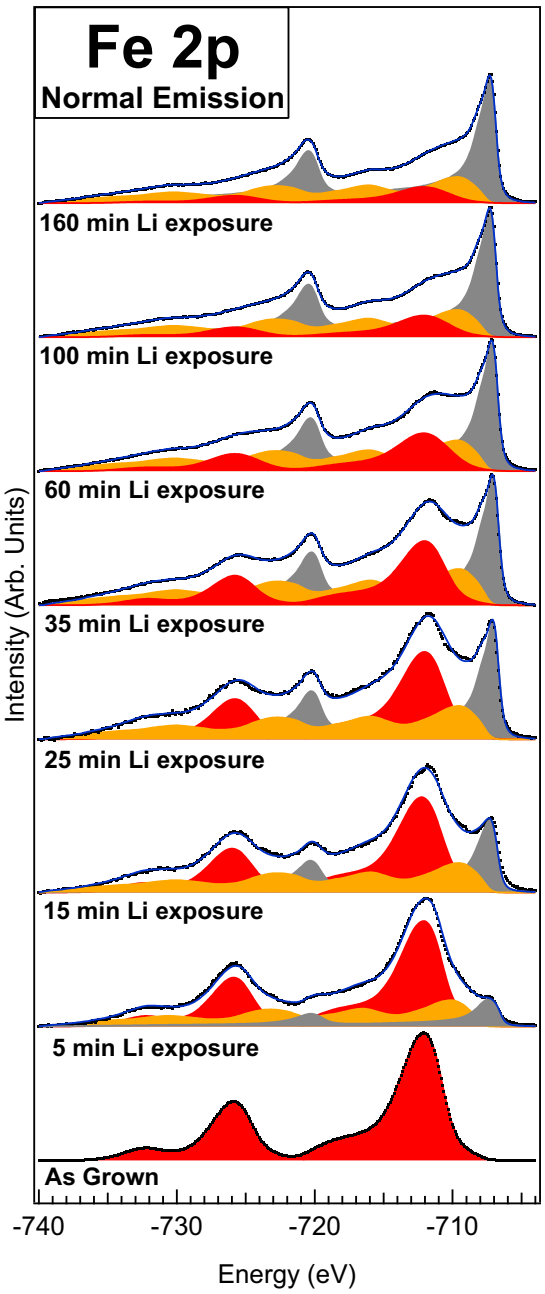

FIG. S4: Fe 2p spectra of the FeF_2 film taken at normal emission after each lithium exposure.

$Fe_xLi_{2-2x}F_2$, (3) thin Fe^0, and (4) thin $Fe_xLi_{2-2x}F_2$. The relative coverages of Fe^0 and $Fe_xLi_{2-2x}F_2$ were determined by the ratio of the specific volume of each species, such that 85% of the surface was covered by $Fe_xLi_{2-2x}F_2$ and 15% by Fe^0. This columnar geometry of overlayer compounds is consistent with the Fe^0 and $Fe_xLi_{2-2x}F_2$ spectral intensities being equal for all angles and overlayer thicknesses.

The FeF_2 signal was then calculated from the following

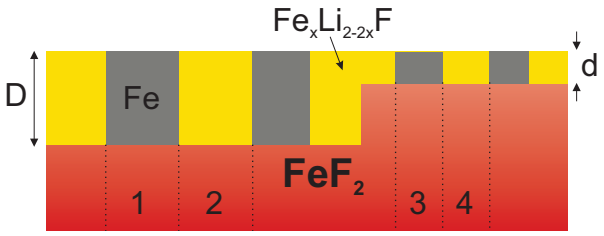

FIG. S5: Model of the Li-FeF_2 conversion reaction used to generate $R(\theta, d)$ curves. The FeF_2 substrate is divided into four distinct regions of overlayer thicknesses and compositions.

equation:[7]

$$I_{\mathrm{FeF_2}}(d,\theta) = I^{\infty}_{\mathrm{FeF_2}} \sum_{i=1}^{4} \Theta_i \left[\exp\left(-\frac{d_i}{\lambda_i(d,\theta)\cos\theta} \right) \right] \quad \text{(S1)}$$

where Θ_i is the fractional coverage of each region and $\lambda_i(d,\theta)$ was calculated for each species, thickness, and emission angle using a procedure described below. Similarly, the Fe^0 and $Fe_xLi_{2-2x}F_2$ signals were then calculated by:

$$I_{\mathrm{Fe}}(d,\theta) = I^{\infty}_{\mathrm{Fe}} \sum_{i=1}^{4} \Theta_i \left[1 - \exp\left(-\frac{d_i}{\lambda_i(d,\theta)\cos\theta} \right) \right]. \quad \text{(S2)}$$

The ratio R was then calculated as

$$R(\theta, d) = \frac{I_{\mathrm{Fe}}(d,\theta)}{I_{\mathrm{FeF_2}}(d,\theta)}. \quad \text{(S3)}$$

The effective attenuation lengths were calculated using the NIST EAL Calculator.[8–11] Table SI shows the EALS calculated at normal emission for each species. Similar tables were calculated at each 5° increment from $0-50°$.

SV. STRUCTURAL PARAMETERS

FeF_2 has a $P4_2/mnm$ rutile (tetragonal) structure with lattice constants $a = b = 4.697$ Å and $c = 3.309$ Å at room temperature. Each Fe^{2+} ion in the bulk is bound to six F^- ions in a distorted octahedral configuration with metal-ion distances of 2.03 Å and 2.10 Å.[12] The FeF_2 [110] channels have nearly square cross sections and are located between the octahedra in the lattice. This square cross section measures 2.10×2.10 Å, from the centers of the fluorine ions at the boundaries. Including the radii of the F^- ions, the cross section of the [110] channel is approximately 0.6 Å, which is smaller than the diameter of either Li^0 or Li^+. This geometrical argument supports the assertion that lithium cannot diffuse into the FeF_2(110) surface. In comparison, the FeF_2 [001] channels are 3.43×3.43 Å from the centers of the bounding ions and 2.18×2.18 Å including the ionic radii, which is large enough to accomodate either Li^0 or Li^+ diffusion.

d (nm)	λ_{FeF_2} (nm)	λ_{Fe} (nm)	$\lambda_{Fe_xLi_{2-2x}F_2}$ (nm)
0.2	1.44	1.04	2.35
0.4	1.42	1.03	2.33
0.6	1.41	1.01	2.32
0.8	1.40	1.01	2.30
1.0	1.40	1.00	2.29
2.0	1.38	0.98	2.26
3.0	1.36	0.96	2.24
4.0	1.35	0.95	2.23
5.0	1.35	0.96	2.22

TABLE SI: Effective attenuation lengths of each iron compound calculated at normal emission using the NIST EAL Database.

Element	Charge	Radius (pm)
Li	0	145
Li	1+	76
F	2-	133
Mg	2+	72
Fe	0	126
Fe	2+	78
Fe	3+	64

TABLE SII: Summary of relevant atomic and ionic radii from Shannon[13] and Slater.[14]

* Fellow, Nanotechnology for Clean Energy IGERT
† Electronic address: bart@physics.rutgers.edu
‡ Current address: Institut Laue-Langevin, 71 avenue des Martyrs, 38000 Grenoble, France

[1] P. C. Graat and M. A. Somers, Applied Surface Science **100**, 36 (1996).
[2] M. Kasrai and D. Urch, J. Chem. Soc., Faraday Trans. 2 **75**, 1522 (1979).
[3] A. Grosvenor, B. Kobe, M. Biesinger, and N. McIntyre, Surf. Interface Anal. **36**, 1564 (2004).
[4] S. Rangan, R. Thorpe, R. A. Bartynski, M. Sina, F. Cosandey, O. Celik, and D. D. T. Mastrigiovanni, The Journal of Physical Chemistry C **116**, 10498 (2012).
[5] J. Ko, K. Wiaderek, N. Pereira, T. Kinnibrugh, J. Kim, P. Chupas, K. Chapman, and G. Amatucci, Appl. Mat. Interfaces **6**, 10858 (2014).
[6] M. Sina, R. Thorpe, S. Rangan, R. Bartynski, G. Amatucci, and F. Consandey, In preparation (2014).
[7] J. F. Watts and J. Wolstenholme, *An Introduction to Surface Analysis by XPS and AES* (2003).
[8] C. Powell and A. Jablonski, *NIST Electron Effective-Attenuation-Lenth Database, Version 1.3, SRD 82* (National Institute of Standards and Technology, Gaithersburg, MD, 2011).

[9] A. Jablonski and C. Powell, Surf. Sci. Rep. **47** (2002).
[10] A. Jablonski and C. Powell, Surf. Sci. **520** (2002).
[11] C. Powell and A. Jablonski, Nucl. Instr. Meth. Phys. Res. **A601** (2009).
[12] J. Stout and S. Reed, J. Am. Chem. Soc. **76**, 5279 (1954).
[13] R. Shannon, Acta Cryst. **A32**, 751 (1976).
[14] J. Slater, J. Chem. Phys. **41** (1964).